Progress In Electromagnetics Research C, Vol. 107, 183–201, 2021

CPW-Fed Dual-Band Compact Yagi-Type Pattern Diversity Antenna for LTE and WiFi

Naveen K. Maurya and Rajarshi Bhattacharya*

Abstract—This paper presents a compact generalized T-shaped printed pseudo-monopole antenna (GeT-PPMA) driven dual-band Yagi-type pattern diversity antenna. In contrary to the common practice, here impedance matching at the lower band is attained by increasing the quality factor (Q) through folding a monopole strip. Afterwards, a GeT-PPMA having relatively lower Q than that of the T-PPMA is proposed. Compared to the simple T-PPMA, the GeT-PPMA has 1.5 times more bandwidth (BW) at the lower band. The dual-band GeT-PPMA is 15.11% more compact than the corresponding straight PPMA (S-PPMA). A highly compact dual-band Yagi-type pattern diversity antenna of size $45.5 \times 63\,\text{mm}^2$, i.e., $0.35\lambda_0 \times 0.48\lambda_0$, where λ_0 is the free space wavelength at the lowest frequency of operation, is designed by using a novel arrangement of two directors and two common folded reflectors. The compactness owes to the folding of the reflectors. The length of the reflector is optimized for providing good front-to-back-ratio (FBR) in the lower band. The length of the two directors is optimized to improve the FBR at the upper band. Usage of the folded reflector is found to degrade the isolation level in the lower band. Near-field analysis is carried out to investigate the mechanism of mutual coupling. Being guided by the near-field study, a $\lambda_g/2$ isolator, where λ_g is the guided wavelength at the lower band, is placed in the gap of the folded reflectors, and the mutual coupling is reduced by about 5 dB.

1. INTRODUCTION

With the evolution of wireless communication at an astonishing rate, there is a constant need for higher data rate and increased reliability in the wireless links. The usage of multiple-input-multiple-output (MIMO) technology and diversity is necessary for attaining these requirements. From an antenna design perspective for modern wireless devices, a MIMO antenna should not only be compact enough, but they require to support different wireless standards, e.g., long-term evolution (LTE), wireless local area network (WLAN), as well [1, 2]. The antenna presented in [2] has much less gain in the backside than the boresight gain due to the comparatively larger ground used in this MIMO microstrip patch antenna. This feature is not suitable for wireless communication, where we do not know the direction of the incoming signal beforehand. Notably, MIMO antennas having pattern diversity results in a lower value of envelope correlation coefficient (ECC) than the other diversity techniques in the indoor Rician channels having a low value of the Rician parameter K [3]. Further, it is worth mentioning that MIMO antennas having Yagi-type pattern diversity perform well even in deep multipath fading scenarios as most of the time two such antenna elements 'see' two different channels. Notably, the antenna reported in [4] is compact, but it is operating at a single band. The work presented in [5] is a multiband antenna, but its feeding structure is not simple and occupies a lot of space. Several Yagi-type MIMO antennas are presented in [6–16]. The quasi-Yagi MIMO antenna of [8] is not compact enough

Received 9 September 2020, Accepted 5 December 2020, Scheduled 14 December 2020
* Corresponding author: Rajarshi Bhattacharya (r.b.1980@ieee.org).
The authors are with the Department of Electronics and Communications Engineering, National Institute of Technology Patna, Patna, Bihar, India.

for modern wireless terminals due to the presence of aperture coupled balun, used to feed the printed dipole antenna, which acts as the driven element in a quasi-Yagi antenna array. Three-element Yagi-type sectoral antennas are reported in [9, 10], which are not compact enough for small wireless terminals as they require a large footprint area. At the same time, the excitation of higher-order loop mode in [10] makes the complete MIMO antenna larger. A compact biplanar MIMO antenna is introduced in [11], where partial pattern diversity is attained as the two 'Yagi-like' antennas produce beams about 40° apart in the azimuthal plane. The compactness of this antenna owes to the simple feeding structure and well-optimized director, placed very close to the driven loop element. Compact single layer Yagi-like MIMO antennas are reported in [12, 13], where a complementary slot reflector (CSR) is used to enhance the directivity of the antenna. A close study reveals that the isolation between the ports of MIMO antennas is on the order of 12 dB and 10 dB in [12] and [13], respectively. A highly compact four-element Yagi-type MIMO antenna is reported in [14], where a meandered dipole element is used as a driven element. Typically, the dipole antenna requires a balun to feed otherwise severe cable current effect that shows up.

To design a compact Yagi-type pattern diversity antenna, we need the driven element to be compact and low in cross-pol level. For example, the compact dual-band antenna, reported in [1], has a high cross-pol level, and hence it cannot be used to drive a Yagi-Uda array. In this work, a dual-band T-shaped printed pseudo-monopole antenna (PPMA), which was introduced in [15], is used as a driven element in the proposed Yagi-type pattern diversity antenna because of its compactness and low cross-pol level. It is interesting to observe that despite the compact size of the T-PPMA itself, the T-PPMA driven dual-band Yagi-type pattern diversity antenna, presented in [15], is not compact at all due to the presence of a long parasitic reflector. Notably, in [17], a T-shaped printed monopole is used in designing an eight-element pattern diversity antenna, but the design supports only single-band operation although a short-circuited stub loading is used to obtain impedance matching in the T-shaped monopole. In conclusion, it could be said that only a few compact dual-band pattern diversity antennas are reported in the literature. Furthermore, Yagi-type MIMO antennas are even rarer. Hence, designing such a dual-band antenna is of considerable interest because of the challenges involved from antenna theoretic perspective and the relevance in the modern wireless communication industry as well.

It is worth mentioning that the structure of the dual-band T-shaped PPMA (T-PPMA), which we work on in this paper, was introduced in [15], but its working principle is explained in this paper. In the context of designing dual-band antenna, here the quality factor (Q) [18] of the lower resonance mode of the T-PPMA is increased through folding the monopolar strip to attain impedance matching at the lower band as well. This folding of the monopolar strip provides a relatively narrowband matching. A flaring is applied to the monopole to increase its bandwidth (BW) in the lower band [19, 20]. Notably, no special matching technique like stub matching is required in this case [20]. In the proposed antenna, which is to be used in modern MIMO software-defined radio (SDR) platforms, pattern diversity is obtained through incorporating dedicated directors and two common reflectors, placed between the two generalized T-PPMAs (GeT-PPMAs). In this work, we reduce the footprint area of the proposed pattern diversity antenna by using a folded reflector [4, 7, 16, 21]. It is pointed out in [16] in the context of single-band PPMA that the usage of folded reflector degrades isolation between elements of the MIMO antenna. This paper provides a solution to this problem and presents a highly compact dual-band Yagi-type pattern diversity antenna incorporating two folded reflectors and an isolator, used to reduce the mutual coupling. Further, a two-step designing approach is adopted for obtaining dual-band Yagi-action. In this approach, the reflector plays a vital role mainly in the lower band whereas the directors improve front-to-back-ratio (FBR) in the upper band. A novel arrangement of directors is introduced as well for improving FBR.

The rest of the paper is organized as follows. Section 2 presents the design of a compact GeT-PPMA. Section 3 describes the design of a single-band Yagi-type MIMO antenna, where the improvement in isolation is achieved by the suppression of E_θ in the near-field region. The design of a dual-band Yagi-type MIMO antenna is presented in Section 4. Concluding remarks are given in Section 5.

2. COMPACT GENERALIZED T-PPMA (GeT-PPMA)

2.1. Obtaining Resonance through Q Enhancement

A straight PPMA (S-PPMA) is designed on a low cost and readily available FR-4 ($\varepsilon_r = 4.4$, $\tan\delta = 0.02$) substrate with a thickness of 1.6 mm to operate at 2.3 GHz LTE band (see Fig. 1(a)). All the antennas presented in this paper are simulated using HFSS full-wave simulator. It is evident from the simulated $[Z_{11}]_{\text{Im}}$ plot of Fig. 2(a) that the straight PPMA is quite capacitive at the lower band, which makes it very difficult to achieve impedance matching. Notably, impedance matching could be obtained by increasing the Q in this case [18]. Hence, the straight PPMA is folded into a T-shape (see Fig. 1(b)) to increase the Q at the lower band through the cancellation effect of the current [7, 15]. We attain 7.59% return-loss (RL) bandwidth (BW) at the 2.3 GHz LTE band. Further, the folding of the strip leads to 26.5% size reduction as well. Fig. 2(a) shows that converting the straight PPMA into T-PPMA to obtain impedance matching at the lower band pushes the Q to a very high value, and we get only 7.59% RLBW at the lower band. To tackle this problem, the central strip of T-PPMA is flared in order to reduce the Q to some extent as shown in Figs. 1(c) and 3(a) [19, 20]. This flared T-PPMA is named as generalized T-PPMA, i.e., GeT-PPMA. As a result of flaring, 1.5 times improvement in RLBW at the lower band is achieved w.r.t the simple T-PPMA as shown in Figs. 2(d) and (e). Notably, flaring has caused the higher band to move a little bit towards lower frequency, but still, it covers the whole upper-WiFi band of 5.2 GHz (see Fig. 2(d)). The fabricated prototype is shown in Fig. 3(a). The S-parameter is measured using Agilent N5222A PNA. Fig. 3(b) shows good agreement between the simulated and measured results of GeT-PPMA.

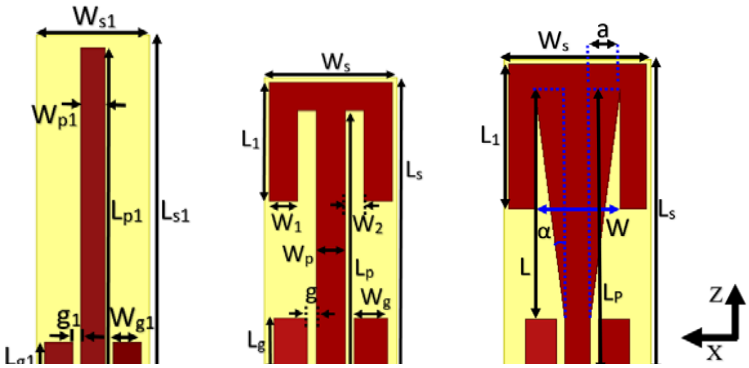

Figure 1. (a) S-PPMA on FR4 board of $\varepsilon_r = 4.4$ and thickness 1.6 mm [Size: $0.551\lambda_g \times 0.18\lambda_g$, where λ_g is calculated at 2.35 GHz]: $L_{g1} = 5$, $W_{g1} = 3.5$, $g_1 = 1$, $L_{p1} = 41.5$, $W_{p1} = 3$, $L_{s1} = 43$, $W_{s1} = 14$, (b) T-PPMA [Size: $0.405\lambda_g \times 0.18\lambda_g$]: $L_g = 6$, $W_g = 3.5$, $g = 1$, $L_p = 28$, $W_p = 3$, $W_1 = 3$, $W_2 = 2$, $L_1 = 12.6$, $L_s = 31.5$ and $W_s = 14$, and (c) GeT-PPMA [Size: $0.469\lambda_g \times 0.218\lambda_g$]: $L_s = 36.5$, $W_s = 17$, $L_1 = 17$, $L = 27$, $W = 10$, $L_p = 33$, $a = 3.5$, $\alpha = 7.39°$ (other dimensions of GeT-PPMA are same to that of T-PPMA) (unit: mm).

2.2. Mode Merger and Excitation of the Hybrid Mode

Figure 2 shows that GeT-PPMA provides more RLBW than the straight PPMA at the upper band due to the merger of two higher-order modes. The presence of kink near unity VSWR point indicates that the higher-order modes combine together at the upper band to give wide RLBW as shown in Figs. 2(b), (c), and (d). The surface current distribution on the antenna is plotted in Fig. 4 in the neighborhood of the second resonance including the frequency 4.2 GHz, which corresponds to the 2nd resonance of the GeT-PPMA shown in Figs. 2(b) and (c). Interestingly, pure 2nd order and 3rd order modes are found to exist at frequencies slightly below and above 4.2 GHz (see Figs. 4(a) and (c)). A close observation of Fig. 4(b) reveals that the surface current distribution at 4.2 GHz on some part of the folded left and

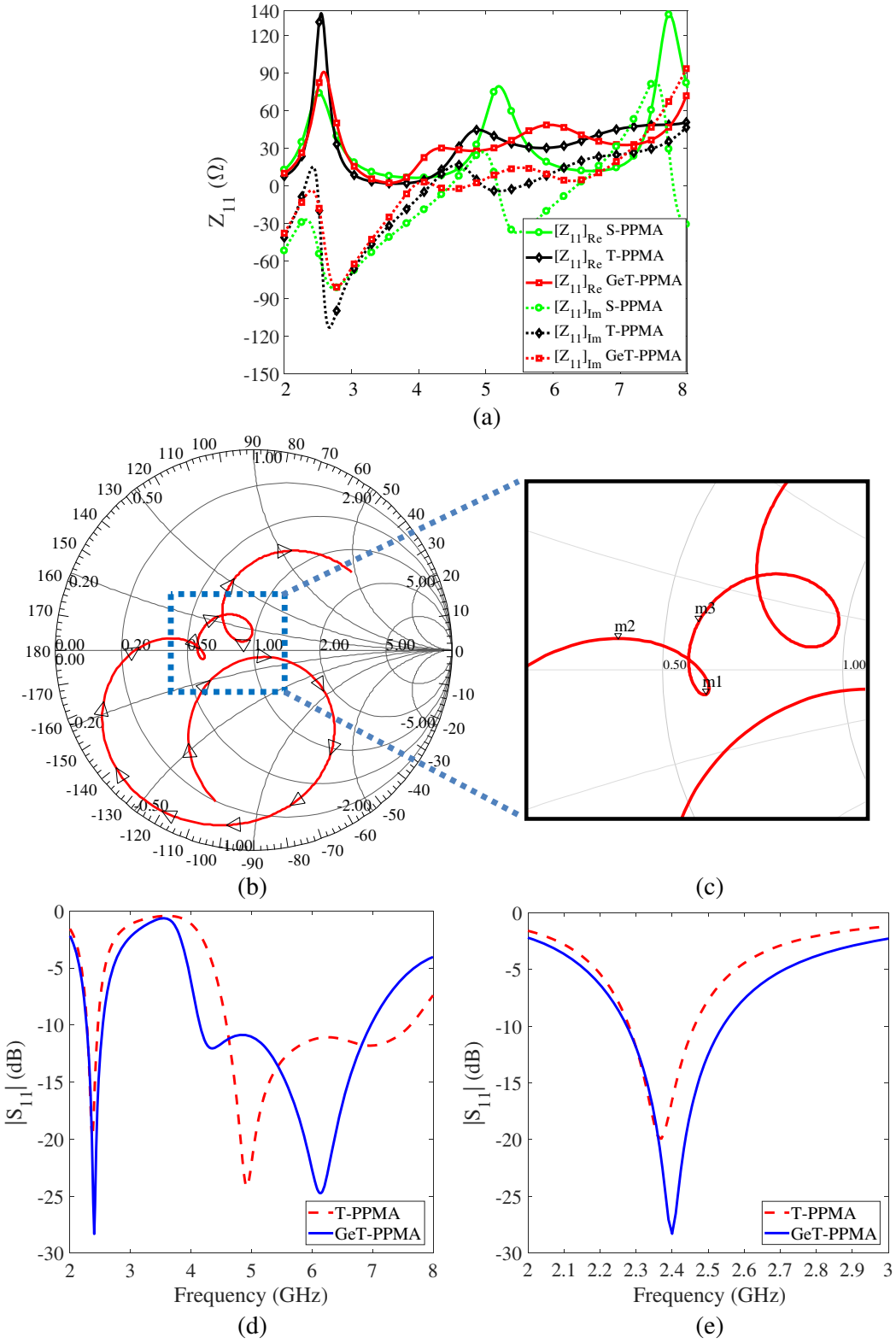

Figure 2. (a) Real and imaginary part of Z_{11}, (b) Z_{in} on the Smith chart of GeT-PPMA, (c) subplot of Smith chart, where $m_2 = 4.05\,\text{GHz}$, $m_1 = 4.2\,\text{GHz}$, and $m_3 = 4.35\,\text{GHz}$, (d) $|S_{11}|$ of T-PPMA and GeT-PPMA, and (e) subplot of $|S_{11}|$ at the lower band depicting T-PPMA offers 180 MHz BW and GeT-PPMA provides 270 MHz BW.

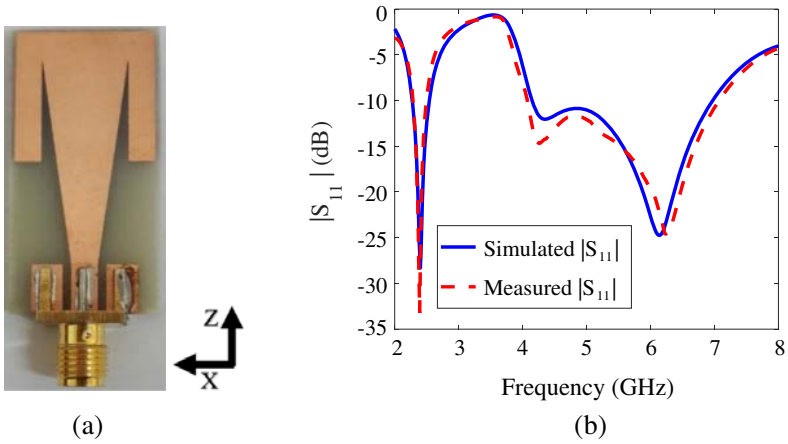

Figure 3. (a) Fabricated prototype and (b) simulated and measured $|S_{11}|$ of GeT-PPMA.

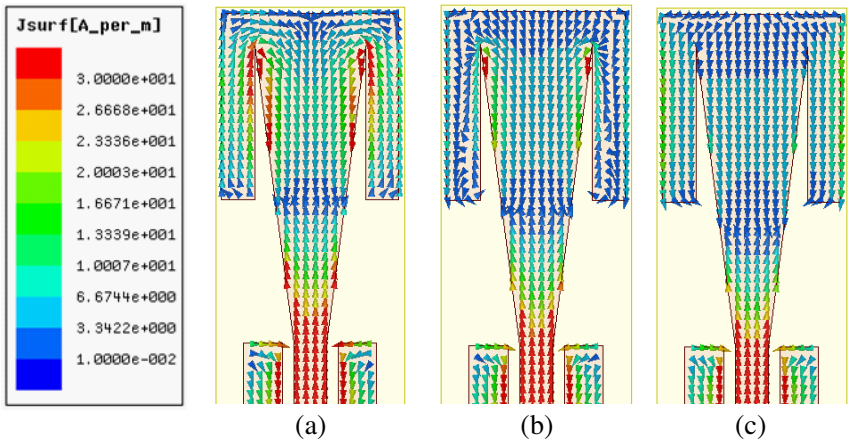

Figure 4. Vector surface current density at (a) 4.05 GHz, (b) 4.2 GHz, and (c) 4.35 GHz.

right arms of the GeT-PPMA is in opposite direction to that of the current distribution of pure 2nd order mode and resembles to be in between pure 2nd order and 3rd order modes.

2.3. Parametric Study

We have carried out three important parametric studies to demonstrate the operating mechanism of the antenna. They also give important design guideline to design a CPW-fed dual-band printed antenna.

2.3.1. Varying the Ratio (L/L_1) Keeping $(L + L_1)$ as Constant

A close observation of the antenna structures, shown in Fig. 5(a), shows that the ratio (L/L_1) is a reasonable metric of the '***extent of folding***' of the arms in the GeT-PPMA. Here, we study the effect of changing the '***extent of folding***' on the antenna characteristics. With this aim, we vary the ratio (L/L_1) while keeping $(L + L_1)$, i.e., the total length of the current path constant at 44 mm. The total length of the current path is kept unaltered to keep the frequency of operation unchanged. It is worth mentioning that all the other parameters of GeT-PPMA are kept unchanged during this parametric study.

As (L/L_1) is decreased from 5.29 to 1.1, the '***extent of folding***' in the GeT-PPMA is increased. The corresponding change in the input impedance (Z_{in}) is plotted on the Smith chart shown in Fig. 5(a). It shows that the quality factor (Q) increases as we increase the '***extent of folding***', and the higher Q

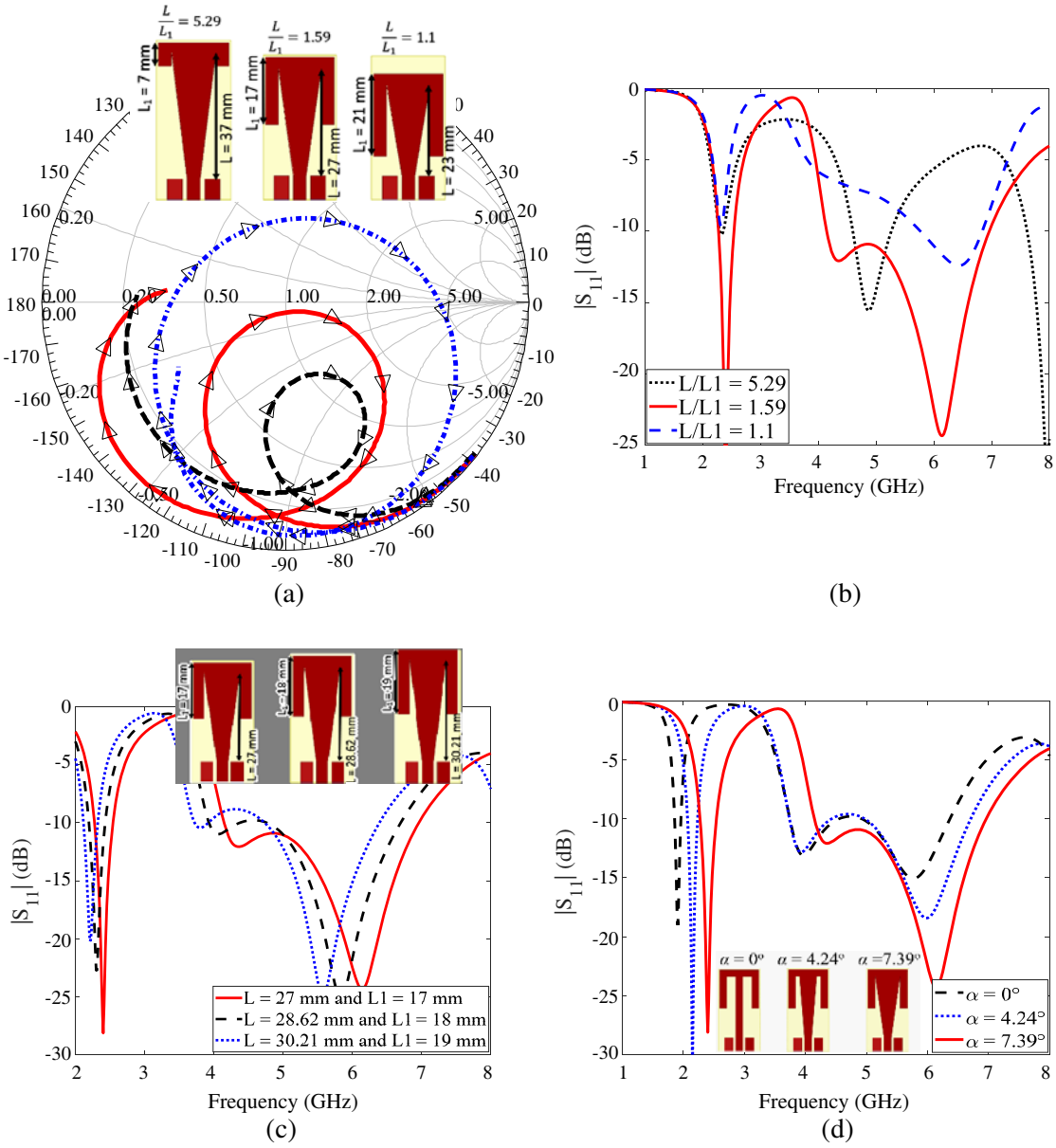

Figure 5. Parametric study: (a) Z_{in} on Smith chart from 1–4 GHz for the different ratio of (L/L_1), keeping $(L + L_1) = 44$ mm as constant, where $(- - - \; L/L_1 = 5.29)$, $(\text{——} \; L/L_1 = 1.59)$, and $(- \cdot - \cdot \; L/L_1 = 1.1)$, (b) $|S_{11}|$ for different values of (L/L_1), keeping $(L + L_1) = 44$ mm as constant, (c) $|S_{11}|$ variation for different values of L and L_1 such that (L/L_1) remains constant at 1.59, and (d) $|S_{11}|$ for different values of the flaring angle α (while keeping all the other parameters unchanged).

value is indicated by the larger size of the circle locus of the Z_{in} on the Smith chart. Fig. 5(a) depicts that lowering (L/L_1) by increasing the folding makes the antenna increasingly inductive. Evidently, the antenna with $(L/L_1) = 5.29$, i.e., minimum folding, is entirely capacitive in the lower band. The antenna structure with $(L/L_1) = 1.1$, i.e., maximum folding is too inductive in the lower band of operation. The final design with $(L/L_1) = 1.59$, i.e., moderate folding, is an optimal one as it approaches the VSWR = 1 point at the band of operation. Fig. 5(b) shows the reflection coefficient at the antenna port. *It is evident that the ratio* (L/L_1) *should be chosen carefully as the matching at the lower band is primarily determined by this factor.*

2.3.2. Varying L and L_1 Keeping (L/L_1) as Constant

In this parametric study, the lengths L and L_1 are increased simultaneously while keeping the ratio (L/L_1), which is a metric of the 'extent of folding' of the GeT-PPMA, constant at 1.59 to vary the total length of the current path (see Fig. 5(c)). In this study, all the other design parameters of GeT-PPMA are kept unchanged. Here, the ratio (L/L_1) is kept unchanged so that the Q value and %BW remain unchanged. Fig. 5(c) shows that the increase in L and L_1 increases the total length of the current path $(L + L_1)$, and the whole frequency band moves to the lower frequency side as a result.

2.3.3. Varying the Flaring Angle

The flaring angle α, indicated in Fig. 1(c), is another important design parameter of GeT-PPMA. In this parametric study, the flaring angle α is varied from 0° (i.e., no flaring) to 7.39° while keeping all the other design parameters unchanged. Fig. 5(d) shows that the increase in α doubles the 10 dB RLBW in the lower band as the BW increases from 104 MHz to 266 MHz [20]. Here, it is worth mentioning that the RLBW at the higher band of GeT-PPMA is very high even for $\alpha = 0°$.

2.4. Radiation Characteristics of GeT-PPMA

The normalized E-plane (ZX) co-polar and cross-polar patterns of the GeT-PPMA are shown in Figs. 6(a) and (b) for 2.35 GHz and 5.25 GHz, respectively. Evidently, the designed antenna has a dipole-like radiation pattern in the E-plane. The cross-polar ratio is found to be about −19.4 dB at 5.25 GHz making it a suitable candidate for Yagi-Uda array. The radiation pattern is measured in a semi-anechoic environment, where a cross-polar component could not be measured. Fig. 6 shows that the measured co-pol component is in agreement with the simulated result.

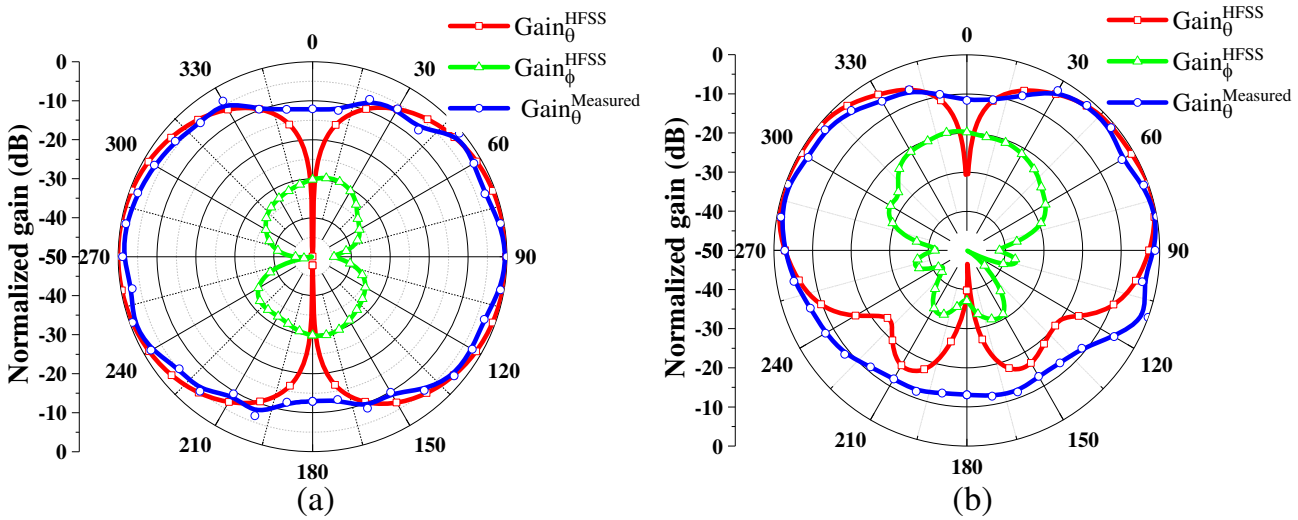

Figure 6. Normalized radiation pattern of GeT-PPMA in ZX-plane at (a) 2.35 GHz and (b) 5.25 GHz.

3. SINGLE BAND YAGI-TYPE PATTERN DIVERSITY ANTENNA HAVING FOLDED REFLECTOR AND ISOLATOR

3.1. Yagi-Type Pattern Diversity Antenna with Straight Reflector

A single band Yagi-type pattern diversity antenna operating at 2.3 GHz LTE band with 7.5% RLBW and 20.5 dB isolation is shown in Fig. 7(a). Here, the two straight PPMAs radiate in two complementary regions of space resulting in pattern diversity [6]. Fig. 7(b) shows that the simulated and measured results are in good agreement.

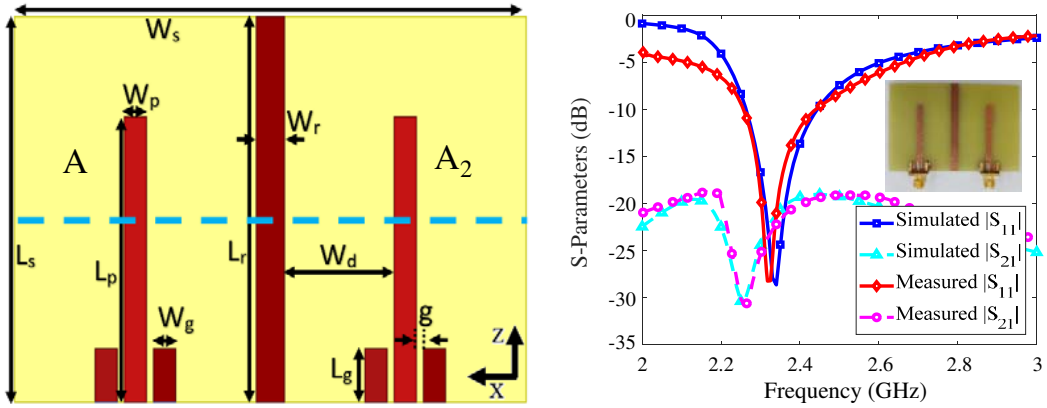

Figure 7. (a) Layout of straight reflector configuration on FR-4 board of $\varepsilon_r = 4.4$ and thickness 1.6 mm (– – is the near-field observation line 3 mm above substrate) [Footprint area: $0.643\lambda_g \times 0.901\lambda_g$]: $L_s = 50$, $W_s = 70$, $L_p = 38$, $W_p = 3$, $L_g = 5$, $W_g = 3$ mm, $L_r = 50$, $W_r = 4$, $W_d = 15$, and $g = 1$ (unit: mm) and (b) simulated and measured S-parameters with the fabricated prototype in inset.

3.2. Yagi-Type Pattern Diversity Antenna with Folded Reflector

It is worth noting that the miniaturization of a Yagi-type pattern diversity antenna requires a length reduction of the reflector, but such reduction is likely to degrade FBR. So, we use a folded reflector to tackle this problem. The pattern diversity antenna with a folded reflector of the total length of 64.75 mm is shown in Figs. 8(a) and (b). As a result of folding, the antenna becomes 18% compact w.r.t the one with a straight reflector. The fabricated prototype is shown in Fig. 8(c). In order to connect reflector along the height of the substrate, the copper tape having conductive adhesive is used. The RLBW and isolation of this antenna have reduced from 7.5% to 5% and 20.5 dB to 17.5 dB, respectively as shown in Fig. 8(d).

3.2.1. The Problem of Near-Field Coupling

It is found that the isolation degrades by 3 dB when the reflector is folded. We study the behavior of the near-field along the width of the substrate on an imaginary line taken 3 mm above the substrate passing through its center as shown in Figs. 8(a) and 10(a) to get better understanding of the physics. It is evident from Fig. 9 that normalized near-field E_θ reaching the 2nd antenna, when port 1 is excited and port 2 terminated in matched load, is more in the case of the folded reflector configuration than the straight reflector configuration case.

3.2.2. The Solution to the Problem of Near-Field Coupling

We introduce a $\lambda_g/2$ long isolator in between the gap of the folded reflector to minimize the near-field coupling between the two PPMAs as shown in Figs. 10(a) and (b). A close observation of Fig. 10(c) reveals that RLBW increases from 5% to 7.56% due to the resonance of the isolator. This antenna provides FBR about 13.62 dB and gain of 6.1 dB at $f = 2.35$ GHz as depicted in Figs. 10(d) and (e), respectively. The cross-polar gain is found to be -29.7 dB down w.r.t co-polar gain. Evidently, the simulated and measured results for both S-parameters and radiation pattern are in good agreement. The ECC, calculated from far-field [2, 22], is found to be only 25.48×10^{-4} at $f = 2.35$ GHz. In this case, we achieve 2 dB improvement in the isolation level w.r.t the case without isolator. It is evident from Fig. 9 that the near-field component reaching 2nd PPMA is quite low as compared to the case without isolator. It is worth noting that the normalized near-E_θ above the isolator is quite high. Therefore, the isolator is reradiating and creating another path for mutual coupling whose phase and amplitude could be controlled by changing the dimension of the isolator to cancel the existing coupling [23].

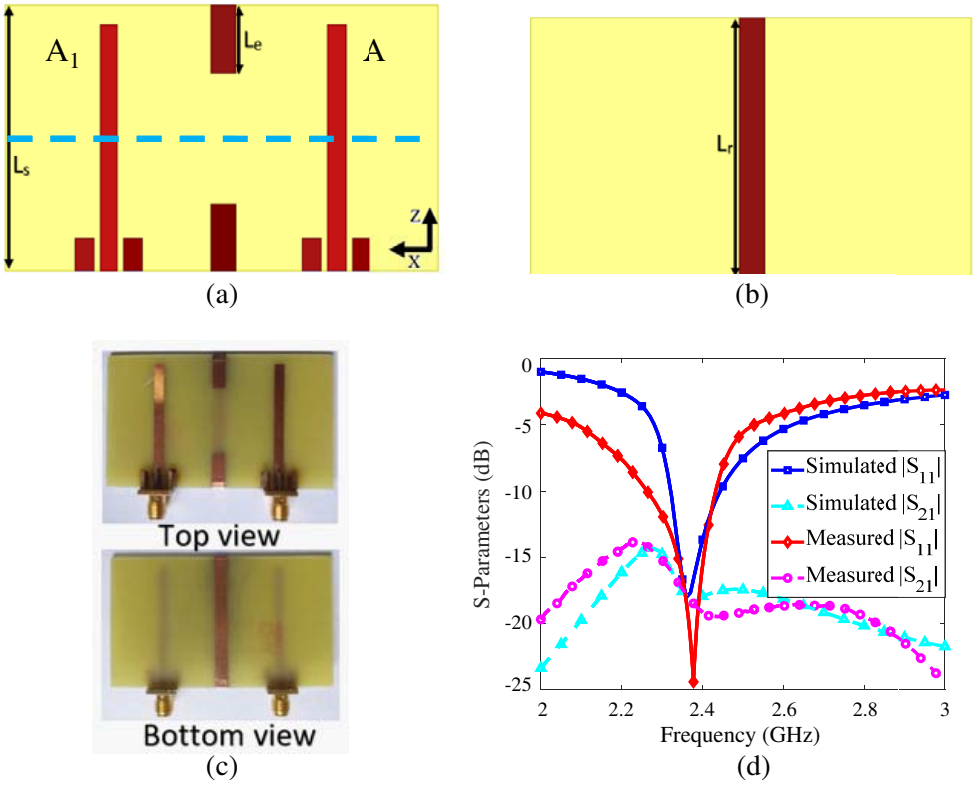

Figure 8. (a) Top view of the layout of folded reflector configuration without isolator on FR-4 board of thickness 1.6 mm (– – is the near-field observation line 3 mm above substrate) [Footprint area: $41 \times 70\,\text{mm}^2$ $(0.527\lambda_g \times 0.901\lambda_g)$]: $L_s = 41$, $L_e = 10.275$, (b) bottom view: $L_r = 41$ (unit: mm), (c) fabricated prototype, and (d) simulated and measured [S].

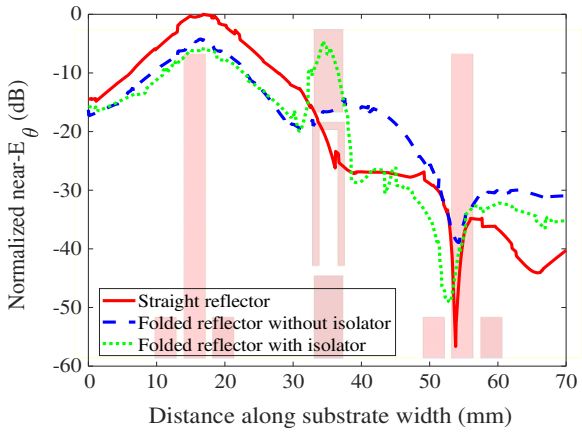

Figure 9. Normalized near-E_θ across the width of the antenna, with port 1 excited and port 2 matched at 2.35 GHz.

4. COMPACT DUAL-BAND YAGI-TYPE PATTERN DIVERSITY ANTENNA

In this section, a compact dual-band Yagi-type pattern diversity antenna is designed using the same approach adopted in designing a single band Yagi-type pattern diversity antenna. In order to get more reliable antenna performance and to make the final antenna less lossy, we use a Rogers 4350B ($\varepsilon_r = 3.66$, $\tan\delta = 0.004$) substrate of 0.762 mm thickness. Here two T-shaped PPMAs are used as

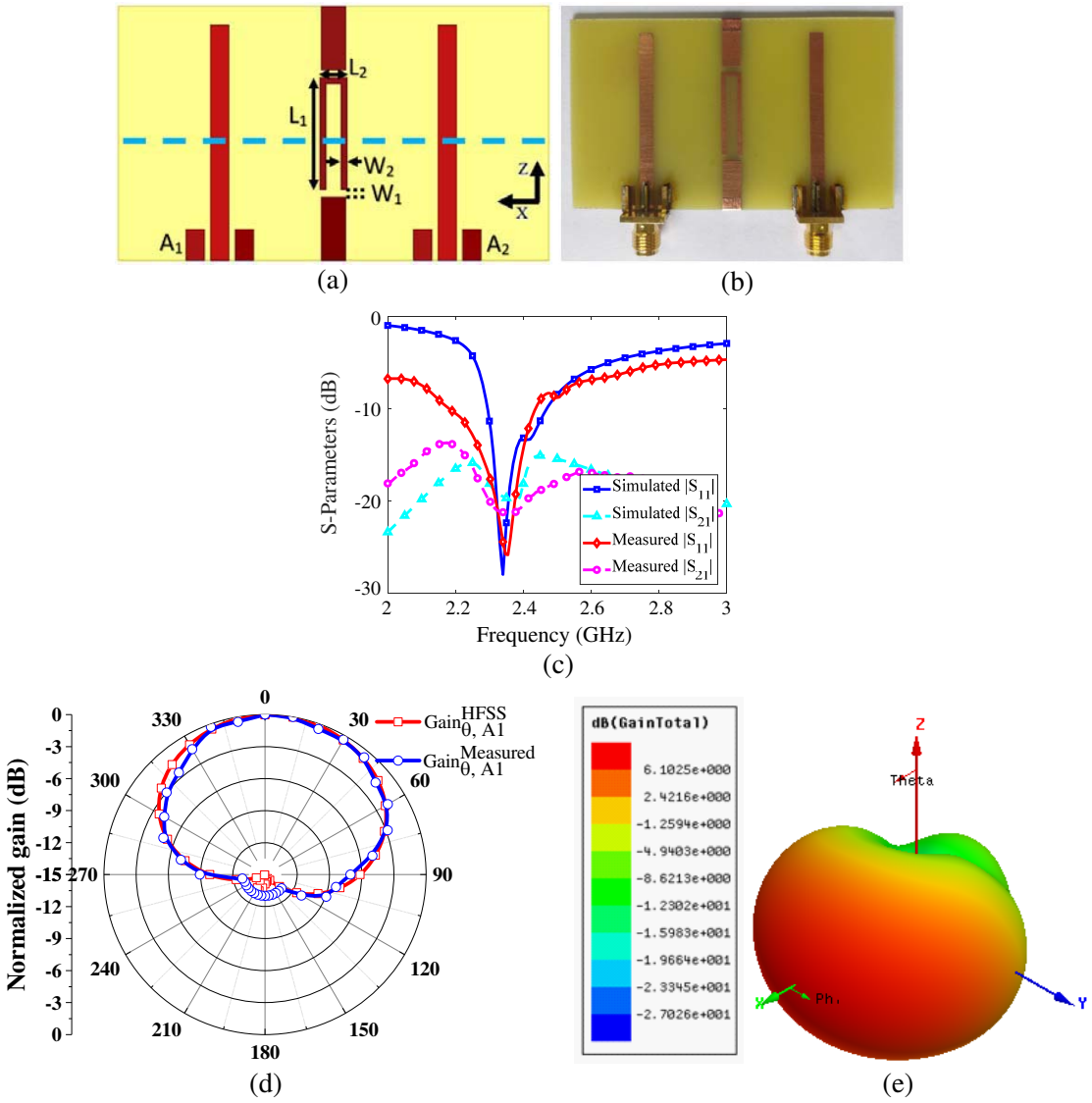

Figure 10. (a) Top view of the layout of folded reflector configuration with isolator on FR-4 board of thickness 1.6 mm (− − is the near-field observation line 3 mm above substrate) [Footprint area: $41 \times 70\,\text{mm}^2$]: $L_1 = 18$, $L_2 = 4.5$, $W_1 = 1.225$, $W_2 = 1$ (unit: mm), (b) fabricated prototype, (c) simulated and measured [S], (d) normalized co-pol radiation pattern in XY-plane at 2.35 GHz, and (e) simulated 3D polar plot at 2.35 GHz when A_1 is excited and A_2 is terminated at matched load.

driven elements for dual-band operation. Notably, the edge-to-edge electrical separation between the two radiating elements becomes much less than the configuration shown in Fig. 10(a) due to the folding of the driven elements (see Fig. 11(a)). This causes isolation to degrade. The following two measures are taken to combat this problem: *i*) the number of reflectors is increased from one to two to reduce mutual coupling through radiation, and *ii*) two MIMO radiating elements are placed anti-symmetrically to increase port-to-port separation as depicted in Figs. 11(a) and (c).

4.1. Two-Step Designing Approach

The design of a wideband/multi-band Yagi-Uda antenna is always a challenging problem, and here we solve this problem in a two-step approach. First, the length of the reflectors is optimized for providing a directive pattern at the lower band, i.e., 2.35 GHz, and we attain FBR of 10.26 dB at this band (see

Fig. 11(e)). The optimized reflector length is found to be 75.02 mm, which is about $2\lambda_g$ at 5.25 GHz, i.e., at the upper band. Evidently, this is too long for providing the required phase shift at the upper band. It leads to FBR of only 6.7 dB at $f = 5.25$ GHz. Next, we incorporate two directors of length $0.374\lambda_g$ each, calculated at $f = 5.25$ GHz, to improve the directive property at the upper band as shown in Figs. 11(a), (c), and (f). Contextually, it is worth noting that no director could be used in the lower band as the director for the lower band will work as a reflector in the higher band. The surface current density of the dual-band pattern diversity antenna at 5.25 GHz is depicted in Fig. 11(b) revealing that there is a null near the center. Hence, the two directors are placed such that the position of the current null is at the gap between the two directors. After insertion of directors, the FBR improves from 6.7 dB to 12.17 dB as shown in Fig. 11(f). The cross-polar gain normalized w.r.t co-polar gain is found less than −31.14 dB and −19.93 dB at 2.35 GHz and 5.25 GHz, respectively as shown in Fig. 11(g). Further, it is worth mentioning that the cross-polar radiation pattern of the Z-directed T-PPMA is similar to

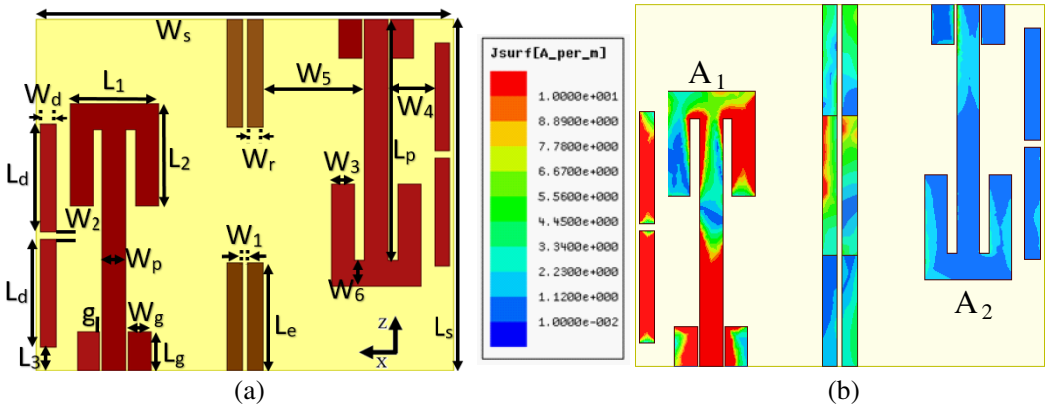

(a) (b)

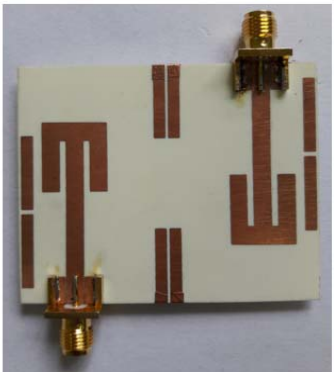

(c)

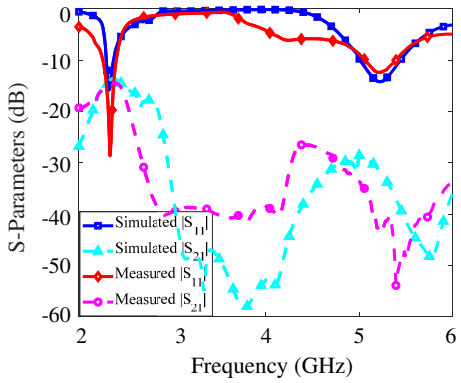

(d)

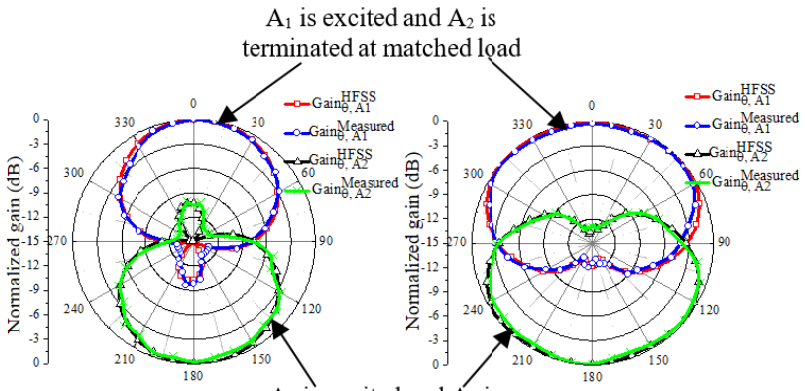

(e) (f)

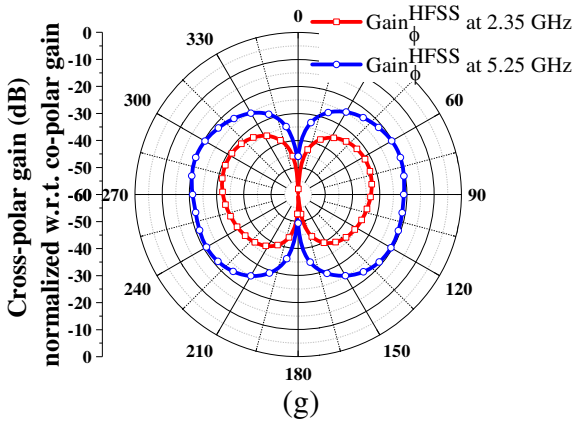

(g)

Figure 11. (a) Top view of the layout of the dual-band folded reflector configuration without isolator on RO4350B board of $\varepsilon_r = 3.66$ and thickness 0.762 mm [Footprint area: $0.544\lambda_g \times 0.645\lambda_g$]: $L_g = 5$, $W_g = 3$, $g = 0.3$, $W_p = 3$, $L_p = 31.2$, $L_3 = 3$, $L_2 = 13.25$, $L_1 = 11.5$, $L_d = 14$, $W_d = 2$, $W_2 = 1$, $W_4 = 6$, $W_3 = 3$, $W_6 = 3.4$, $W_r = 2$, $L_e = 14$, $W_5 = 13.2$, $W_1 = 0.6$, $W_s = 54$, $L_s = 45.5$ (unit: mm), (b) surface current density at 5.25 GHz when A_1 is excited and A_2 is terminated at matched load, (c) fabricated prototype, (d) simulated and measured [S], simulated and measured normalized G_θ in XY-plane (e) at 2.35 GHz, (f) at 5.25 GHz, and (g) simulated G_ϕ in XY-plane.

the co-polar radiation pattern of an X-oriented dipole, and for this MIMO configuration, the reflectors are oriented along Z-axis. Hence, we do not get any Yagi action on cross-polar radiation.

In this work, we optimize the dual-band Yagi-Uda antenna without getting involved in the process of simulation intensive optimization, which is generally accomplished using evolutionary algorithms (EAs) [24–26]. Figs. 12(a) and 13(a) show that the FBR of the lower band (FBR_{LF}) has a high sensitivity to the variation of the design parameters of the reflectors, whereas it has hardly any sensitivity to the design parameters of the directors. In the same way, the higher band FBR (FBR_{HF}) shows high sensitivity to the variation of the design parameters of the directors, whereas it has hardly any sensitivity to the design parameters of the reflectors (see Figs. 12(b) and 13(b)). Therefore, it is concluded that the reflector plays a vital role mainly in the lower band, whereas the directors improve front-to-back-ratio (FBR) in the upper band. Figs. 12 and 13 are generated for the dual-band T-PPMA driven Yagi-type pattern diversity antenna without an isolator (see Fig. 11(a)). Hence, in the first step, we do not incorporate any director in the design and optimize the Yagi-type pattern diversity antenna at the lower

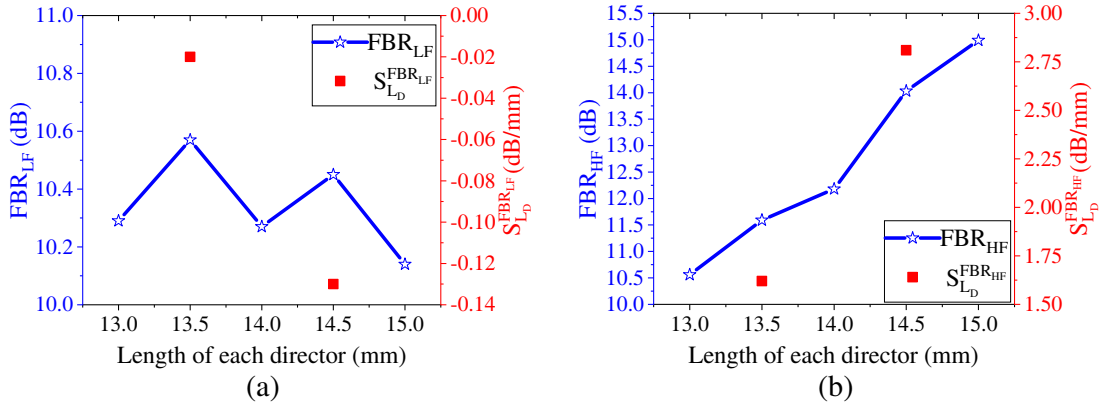

(a) (b)

Figure 12. FBR and sensitivity w.r.t variation in the length of the director at (a) 2.35 GHz and (b) 5.25 GHz, where $S_{L_D}^{FBR_{LF}} = \frac{\partial FBR_{LF}}{\partial L_D}\Big|_{L_D=L_{D_0}}$, and $S_{L_D}^{FBR_{HF}} = \frac{\partial FBR_{HF}}{\partial L_D}\Big|_{L_D=L_{D_0}}$.

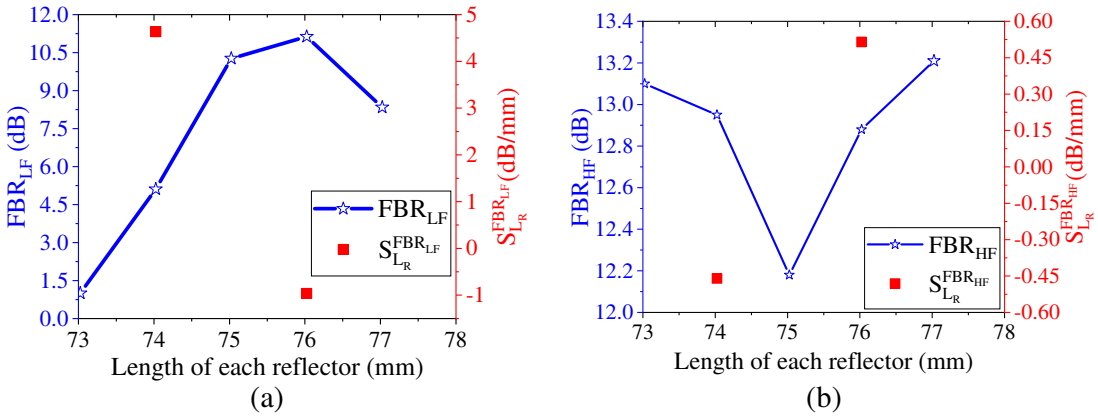

Figure 13. (a) FBR and sensitivity w.r.t variation in the length of reflector at (a) 2.35 GHz and (b) 5.25 GHz, where $S_{L_R}^{FBR_{LF}} = \frac{\partial FBR_{LF}}{\partial L_R}\Big|_{L_R=L_{R_0}}$, and $S_{L_R}^{FBR_{HF}} = \frac{\partial FBR_{HF}}{\partial L_R}\Big|_{L_R=L_{R_0}}$.

band by optimizing the parameters of the common reflectors. In the next step, we introduce a pair of directors and optimize the performance of the Yagi-Uda antenna at the upper band while keeping the position and size of the reflector unchanged. In the final step, the Yagi-type dual-band pattern diversity antenna is fine-tuned to meet all the desired performance metrics. Thus, in this two-step design process, the dual-band MIMO antenna is manually optimized using a fewer number of the parametric sweep of HFSS as we handle a smaller number of design variables at a time.

4.2. Study on Gain Saturation

Here, we present a study on the gain saturation of a Yagi-type pattern diversity antenna without an isolator. In this study, the number of reflectors is not altered. Instead, the number of directors is increased from 1 pair to 4 pairs as depicted in Fig. 14(a). Fig. 14(b) shows that the gain at the lower band is insensitive to the number of directors and that in turn justifies our argument given in the favor of the proposed two-step designing approach of the dual-band Yagi antenna, presented in Section 4.1. The highest attainable gain in the 5.25 GHz band is about 7.72 dBi, but we attain it at the cost about 33% increase in antenna footprint area. The total size of the antenna shown in Fig. 14(a) is $45.5 \times 72\,\text{mm}^2$. However, it is worth noting that even the larger high gain antenna could be fit into a WiFi access point.

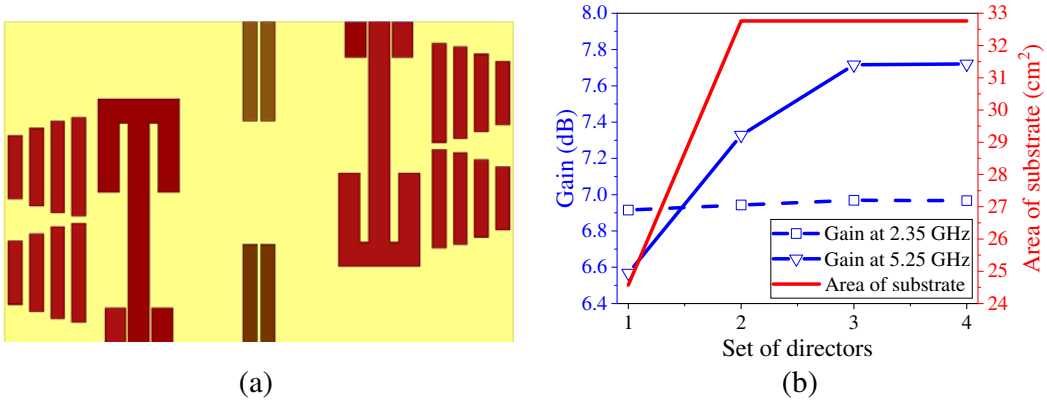

Figure 14. (a) MIMO antenna with four pairs of directors and (b) corresponding gain and area of the substrate vs the number of the set of directors of the MIMO antenna.

4.3. Incorporation of the Isolator

Figure 11(d) shows that the isolation between two MIMO elements is quite good in the upper band. However, the isolation is only 13.5 dB in the lower band as the electrical separation between the two antennas is less at a lower frequency. So, we design a half-wavelength long isolator and insert it to the gap of the reflector as shown in Figs. 15(a) and (b) resulting in improvement of the isolation level from 13.5 dB to 18 dB as shown in Fig. 15(c). The dual-band MIMO antenna has a 10 dB RLBW of 3.44% and 7.26% in the lower and upper bands, respectively. FBRs of 10.15 dB and 13 dB are attained at $f = 2.35$ GHz and 5.25 GHz, respectively. Figs. 11(e) and (f) show the radiation patterns generated by A_1 when A_2 is terminated at matched load occupying complementary regions in space. It is further observed that the insertion of an isolator has a negligible effect on the antenna radiation pattern. The ECC is computed from radiated far-field, and it is found to be only 6.8×10^{-3} and 1.3×10^{-5} in the lower and upper bands, respectively.

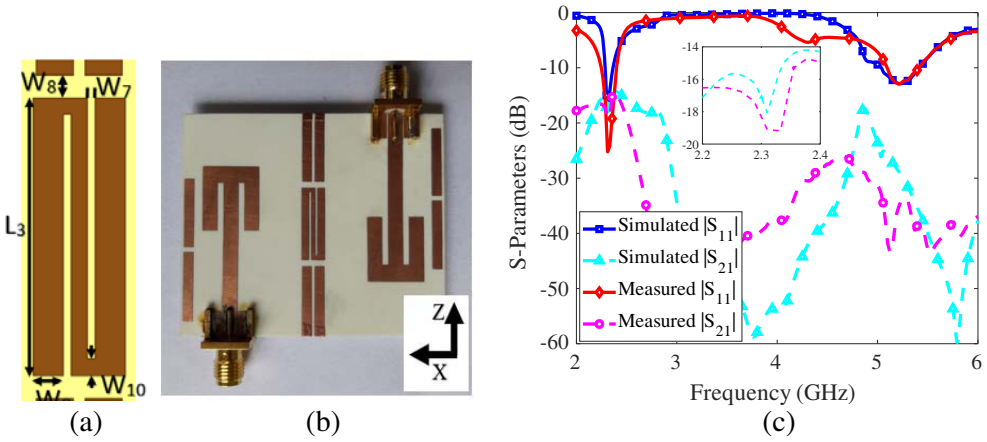

Figure 15. (a) Layout of the isolator [Footprint area of antenna: $0.544\lambda_g \times 0.645\lambda_g$]: $L_3 = 15$, $W_7 = 0.4$, $W_8 = 1.25$, $W_9 = 1.6$, $W_{10} = 0.9$, (unit: mm), (b) fabricated prototype of the dual-band MIMO antenna with isolator on RO4350B board, and (c) simulated and measured [S].

Finally, in order to improve the RLBW in the lower band, the GeT-PPMA is used as a driven element in the dual-band Yagi-type pattern diversity antenna with isolator configuration as shown in Figs. 16(a) and (b). This leads to 1.39 times improvement in the RLBW w.r.t simple T-PPMA as a driven element as shown in Fig. 16(c). In this case, an isolator helps to achieve about 5 dB improvement in the isolation at the lower band. The simulated and measured S-parameters are in good agreement. The gains of the proposed antenna are 6.87 dB and 7.7 dB, whereas FBRs are 12.58 dB and 16.64 dB at 2.35 GHz and 5.25 GHz, respectively. The cross-polar gain normalized w.r.t co-polar gain is found less than -25.81 dB and -17.82 dB at 2.35 GHz and 5.25 GHz, respectively. The ECC is computed from radiated far-field, and it is found to be only 5.67×10^{-3} and 1.29×10^{-5} in the lower and upper bands, respectively. The radiation efficiency of the proposed MIMO antenna is shown in Fig. 16(f). A close agreement between simulated and measured radiation efficiencies is found with peak measured efficiency of 95.33% at 5.4 GHz.

Table 1 provides a detailed performance comparison of this work with [15]. Evidently, the GeTPPMA based solution outperforms the one presented in [15] almost in every aspect. For the antenna presented in [15], the FBRs are 8.25 and 5.9 dB at the lower and upper bands, respectively. It is worth noting that we have achieved FBR better than 10 dB at both bands in the case of the GeT-PPMA based Yagi-type pattern diversity antenna.

Performance comparison of the proposed antenna with recently published MIMO antennas is presented in Table 2. Table 2 depicts that the proposed antenna has better ECC than the one in [2]. Further, as discussed in the introduction, the antenna presented in [2] has an issue that it would provide little sensitivity to signals coming from the backside. It is worth mentioning that the works presented in [8–14] are either wideband or single band antenna with a Yagi-type radiation pattern. The proposed

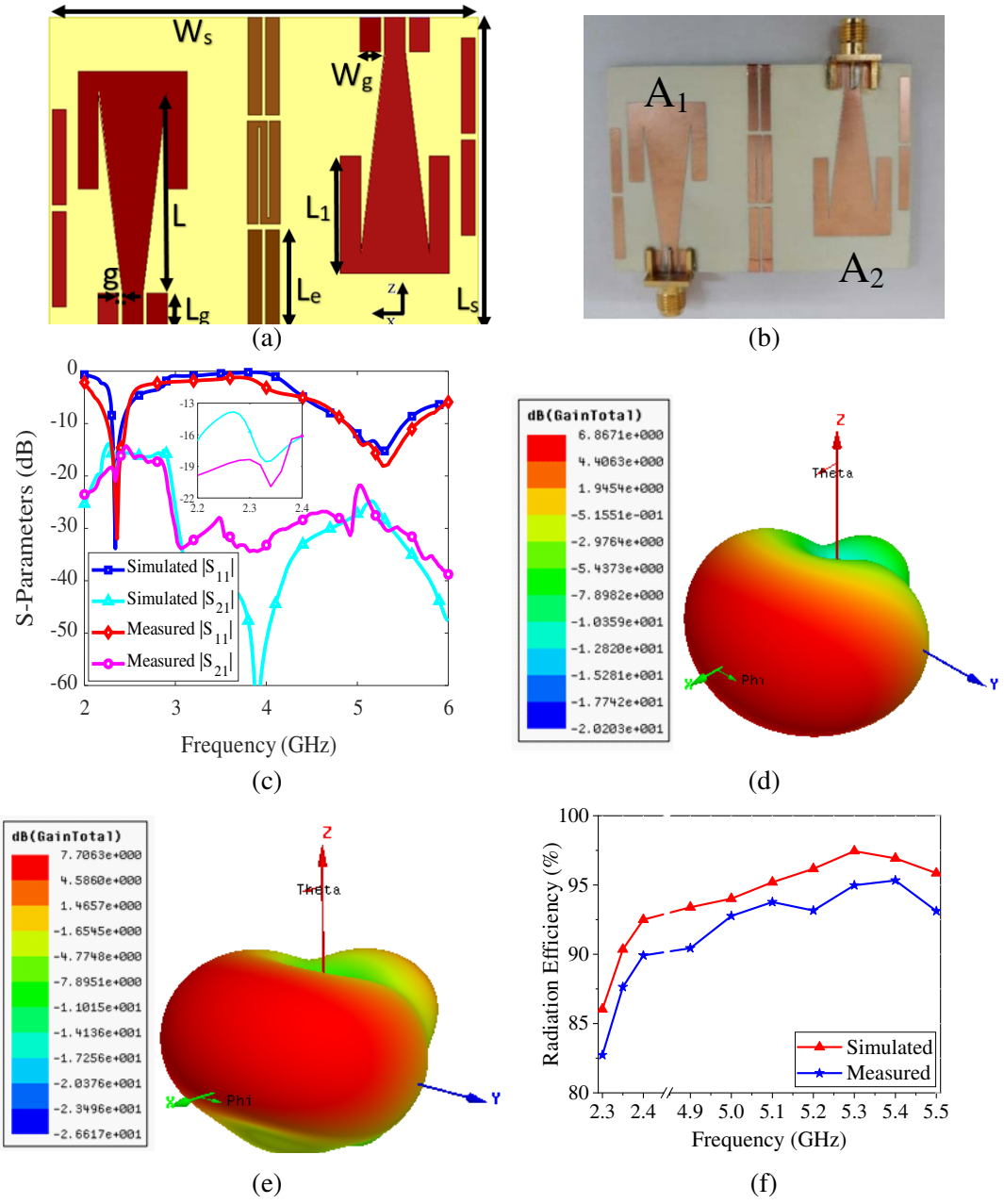

Figure 16. (a) Proposed MIMO antenna [Footprint area of antenna: $0.544\lambda_g \times 0.754\lambda_g$]: $L_s = 45.5$, $W_s = 63$, $L_e = 14.3$, $L_1 = 17.2$, $L = 29.6$, $L_g = 5$, $W_g = 3$, $g = 0.6$, (unit: mm), (b) fabricated prototype on RO4350B board, (c) simulated and measured [S], 3D polar plot at (d) 2.35 GHz, (e) 5.25 GHz when A_1 is excited and A_2 is terminated at matched load, and (f) simulated and measured radiation efficiency.

low-profile compact dual-band antenna has Yagi-type pattern diversity with a complementary radiation pattern, which has been revealed by a thorough literature survey to be very rarely achieved so far. It is important to note that the presence of surrounding closely spaced dielectric and metallic elements causes a loading effect on the MIMO antenna, and this loading may potentially increase the similarity of radiation patterns of the MIMO elements. Hence, it is desirable to make the element radiation patterns orthogonal as well in the case of the antennas, where the MIMO patterns are partially orthogonal as they do not occupy the complementary regions of the space. In this respect, the proposed antenna has an advantage over many dual-band pattern diversity antennas, available in the literature. Overall, the

Table 1. Comparative study.

S. No.	Parameters	[15]	This Work with T-PPMA	This Work with GeT-PPMA
1	Total Size ($\lambda_0^{\dagger}$) (Single Element)	$0.25\lambda_0 \times 0.093\lambda_0$ ($51 \times 19\,\text{mm}^2$)	$0.24\lambda_0 \times 0.11\lambda_0$ ($31.5 \times 14\,\text{mm}^2$)	$0.28\lambda_0 \times 0.13\lambda_0$ ($36.5 \times 17\,\text{mm}^2$)
2	Fractional BW (%) (Single Element)	5.4, 54	7.59, 49.75	11.22, 50.72
3	Total Size ($\lambda_0^{\dagger}$) (MIMO)	$0.48\lambda_0 \times 0.3\lambda_0$ ($100 \times 62\,\text{mm}^2$)	$0.35\lambda_0 \times 0.41\lambda_0$ ($45.5 \times 54\,\text{mm}^2$)	$0.35\lambda_0 \times 0.48\lambda_0$ ($45.5 \times 63\,\text{mm}^2$)
4	Fractional BW (%) (MIMO)	2.04, 53.14	3.44, 7.26	4.96, 12.12
5	Gain (dBi) (MIMO)	6.25, 6.53	6.86, 7.25	6.87, 7.7
6	FBR (MIMO)	8.25, 5.9	10.15, 13	12.58, 16.64
7	ECC (far-field)	1.53×10^{-2}, 9.5×10^{-2}	6.8×10^{-3}, 1.3×10^{-5}	5.67×10^{-3}, 1.29×10^{-5}

$^{\dagger}\lambda_0$ is the free-space wavelength at the lowest operating frequency

proposed antenna is found to provide the lowest ECC in spite of having a compact size. At the same time, the proposed antenna has good gain, radiation efficiency, and port-level isolation all together at both the bands as compared to other works in Table 2.

Table 2. State-of-the-art comparison.

References & Antenna Type	Total Size ($\lambda_0 \times \lambda_0$)†	Bandwidth (GHz)	Min. Isolation (dB)	Max. ECC‡	Radiation Efficiency (%)	Gain (dBi)
[2]: Dual-band Pattern/Polarization Diversity (Four-Element MIMO)	0.41×0.41	3.47–3.52, 5.67–5.73	18.4, 22.7	0.08	63, 65	2.7, 2.85
[8]: Wideband Quasi-Yagi Pattern Diversity (Two-Element MIMO)	1.82×0.86	7–13.8	26	-	-	3.2 to 7.8
[9]: Sectoral Quasi-Yagi Pattern Diversity (Three-Element MIMO)	0.94×0.82	5.15–5.35	-	-	-	6 Directivity
[10]: Wideband Sectoral Quasi-Yagi Pattern Diversity (Three-Element MIMO)	$3.67\lambda_0^2$ (Area)	5.4–6.35	28	0.012	> 90	5
[11]: UWB Yagi-Type Pattern Diversity (Two-Element MIMO)	0.69×1.11	4.18–6.58	17	0.0568	> 80 Total Eff.	> 6

[12]: Slot Based Yagi-Type MIMO (Two-Element MIMO)	0.46×0.93	3.48–3.8	12	0.0385	73	> 4.3 Realized Gain
[13]: Orthogonally Polarized Yagi-Type MIMO (Four-Port MIMO)	0.38×0.97	3.26–3.88	10	0.0928	> 75 Total Eff.	4 Realized Gain
[14]: Broadband Yagi-Type Pattern Diversity (Four-Element MIMO)	0.68×0.68	2.32–2.95	14	N.A.	> 83	3–5.5
[15]: Dual-band Yagi-Type Pattern Diversity (Two-Element MIMO)	0.48×0.3	1.44–1.5, 3.35–5.9	24	0.095	94.81, 97.12	6.25, 6.53
Proposed Dual-band Yagi-Type Pattern Diversity (Two-Element MIMO)	0.35×0.48	2.3–2.417, 4.88–5.51	15.68, 24.8	**0.0056**	90.35, 96.49	**6.87, 7.7**

[†] λ_0 is the free-space wavelength at the lowest operating frequency
[‡] ECC is envelope-correlation-coefficient calculated from far-field

5. CONCLUSION

A compact dual-band Yagi-type pattern diversity antenna has been designed using two common folded reflectors, optimized for the lower band. An isolator has been designed accordingly to improve the isolation level in the lower band. Further, a new arrangement of directors has been introduced, and director length has been optimized to improve FBR at the upper band. Both the $|S_{21}|$ and ECC are found to be quite good making the designed antenna suitable for diversity application in multi-path rich wireless channels.

ACKNOWLEDGMENT

This work is supported by the Young Faculty Research Fellowship (YFRF) reference No: DIC/MUM/GA/10 (37)D of MeitY, Govt. of India.

REFERENCES

1. Dioum, I., A. Diallo, S. M. Farssi, and C. Luxey, "A novel compact dual-band LTE antenna-system for MIMO operation," *IEEE Transactions on Antennas and Propagation*, Vol. 62, No. 4, 2291–2296, 2014,
2. Boukarkar, A., X. Q. Lin, Y. Jiang, L. Y. Nie, P. Mei, and Y. Q. Yu, "A miniaturized extremely close-spaced four-element dual-band MIMO antenna system with polarization and pattern diversity," *IEEE Antennas and Wireless Propagation Letters*, Vol. 17, No. 1, 134–137, 2018.
3. Dietrich, C. B., K. Dietze, J. R. Nealy, and W. L. Stutzman, "Spatial, polarization, and pattern diversity for wireless handheld terminals," *IEEE Transactions on Antennas and Propagation*, Vol. 49, No. 9, 1271–1281, 2001.

4. Juan, Y., W. Che, Z. N. Chen, and W. Yang, "A longitudinally compact Yagi-Uda antenna with a parasitic interdigital strip," *IEEE Antennas and Wireless Propagation Letters*, Vol. 16, 2618–2621, 2017.
5. Alekseytsev, S. A. and A. P. Gorbachev, "The novel printed dual-band quasi-Yagi antenna with end-fed dipole-like driver," *IEEE Transactions on Antennas and Propagation*, Vol. 68, No. 5, 4088–4090, 2020.
6. Bhattacharya, R., R. Garg, and T. K. Bhattacharyya, "A compact Yagi-Uda type pattern diversity antenna driven by CPW-fed pseudomonopole," *IEEE Transactions on Antennas and Propagation*, Vol. 64, No. 1, 25–32, 2016.
7. Bhattacharya, R., R. Garg, and T. K. Bhattacharyya, "Design of a PIFA-driven compact Yagi-type pattern diversity antenna for handheld devices," *IEEE Antennas and Wireless Propagation Letters*, Vol. 15, 255–258, 2016.
8. Gu, L., Y.-W. Zhao, Q.-M. Cai, and Z.-P. Zhang, "Wideband quasi-Yagi antenna design and its usage in MIMO/diversity applications," *Progress In Electromagnetics Research C*, Vol. 71, 33–40, 2017.
9. Capobianco, A., F. M. Pigozzo, A. Assalini, M. Midrio, S. Boscolo, and F. Sacchetto, "A compact MIMO array of planar end-fire antennas for WLAN applications," *IEEE Transactions on Antennas and Propagation*, Vol. 59, No. 9, 3462–3465, 2011.
10. Jehangir, S. S. and M. S. Sharawi, "A wideband sectoral quasi-Yagi MIMO antenna system with multibeam elements," *IEEE Transactions on Antennas and Propagation*, Vol. 67, No. 3, 1898–1903, 2019.
11. Jehangir, S. S. and M. S. Sharawi, "A miniaturized UWB biplanar Yagi-like MIMO antenna system," *IEEE Antennas and Wireless Propagation Letters*, Vol. 16, 2320–2323, 2017.
12. Jehangir, S. S. and M. S. Sharawi, "A single layer semi-ring slot Yagi-like MIMO antenna system with high front-to-back ratio," *IEEE Transactions on Antennas and Propagation*, Vol. 65, No. 2, 937–942, 2017.
13. Jehangir, S. S. and M. S. Sharawi, "A compact single-layer four-port orthogonally polarized Yagi-like MIMO antenna system," *IEEE Transactions on Antennas and Propagation*, Vol. 68, No. 8, 6372–6377, 2020.
14. Ding, K., C. Gao, D. Qu and Q. Yin, "Compact broadband MIMO antenna with parasitic strip," *IEEE Antennas and Wireless Propagation Letters*, Vol. 16, 2349–2353, 2017.
15. Maurya, N. K. and R. Bhattacharya, "CPW-fed dual-band pseudo-monopole antenna for LTE/WLAN/WiMAX with its usage in MIMO," *2016 IEEE International Symposium on Antennas and Propagation (APSURSI)*, 455–456, Fajardo, 2016.
16. Maurya, N. K., M. Tulsyan, R. Bhattacharya, and A. Kumar, "Design and near field analysis of compact CPW-fed printed pseudo-monopole driven Yagi-type pattern diversity antenna," *2017 IEEE Applied Electromagnetics Conference (AEMC)*, 1–2, Aurangabad, 2017.
17. Ding, C. F., X. Y. Zhang, C. Xue, and C. Sim, "Novel pattern-diversity-based decoupling method and its application to multielement MIMO antenna," *IEEE Transactions on Antennas and Propagation*, Vol. 66, No. 10, 4976–4985, Oct. 2018.
18. Obeidat, K. A., B. D. Raines, and R. G. Rojas, "Discussion of series and parallel resonance phenomena in the input impedance of antennas," *Radio Science*, Vol. 45, No. 06, 1–9, 2010.
19. Chen, Z. N., M. J. Ammann, X. Qing, X. H. Wu, T. S. P. See, and A. Cai, "Planar antennas," *IEEE Microwave Magazine*, Vol. 7, No. 6, 63–73, 2006.
20. Balanis, C. A., *Antenna Theory Analysis and Design*, 3rd Edition, 497–541, John Wiley and Sons, United Kingdom, 2005.
21. Rezaeieh, S. A., M. A. Antoniades, and A. M. Abbosh, "Miniaturized planar Yagi antenna utilizing capacitively coupled folded reflector," *IEEE Antennas and Wireless Propagation Letters*, Vol. 16, 1977–1980, 2017.

22. Mikki, S. M. and Y. M. M. Antar, "On cross correlation in antenna arrays with applications to spatial diversity and MIMO systems," *IEEE Transactions on Antennas and Propagation*, Vol. 63, No. 4, 1798–1810, 2015.
23. Minz, L. and R. Garg, "Reduction of mutual coupling between closely spaced PIFAs," *Electronics Letters*, Vol. 46, No. 6, 392–394, 2010.
24. Grout, V., M. O. Akinsolu, B. Liu, P. I. Lazaridis, K. K. Mistry, and Z. D. Zaharis, "Software solutions for antenna design exploration: A comparison of packages, tools, techniques, and algorithms for various design challenges," *IEEE Antennas and Propagation Magazine*, Vol. 61, No. 3, 48–59, 2019.
25. Bhattacharya, R., T. K. Bhattacharyya, and R. Garg, "Position mutated hierarchical particle swarm optimization and its application in synthesis of unequally spaced antenna arrays," *IEEE Transactions on Antennas and Propagation*, Vol. 60, No. 7, 3174–3181, 2012.
26. Cao, Y., H. Zhang, W. Li, M. Zhou, Y. Zhang, and W. A. Chaovalitwongse, "Comprehensive learning particle swarm optimization algorithm with local search for multimodal functions," *IEEE Transactions on Evolutionary Computation*, Vol. 23, No. 4, 718–731, 2019.